remote sensing

MDPI

Article

Rainfall Differences and Possible Causes of Similar-Track Tropical Cyclones Affected and Unaffected by Binary Tropical Cyclones (BTCs) in China

Mingyang Wang [1,2], Fumin Ren [2,*], Guanghua Chen [3] and Xiaohong Lin [4,5]

[1] Key Laboratory of Meteorological Disaster, Ministry of Education (KLME), Nanjing University of Information Science and Technology, Nanjing 210044, China; bboywangmingyang@hotmail.com
[2] State Key Laboratory of Severe Weather, Chinese Academy of Meteorological Sciences, Beijing 100081, China
[3] Key Laboratory of Cloud-Precipitation Physics and Severe Storms, Institute of Atmospheric Physics, Chinese Academy of Sciences, Beijing 100029, China; cgh@mail.iap.ac.cn
[4] Fujian Provincial Key Laboratory of Hazardous Weather, Fuzhou 350028, China; pop_lxh@163.com
[5] Fujian Meteorological Observatory, Fuzhou 350028, China
* Correspondence: fmren@163.com

Abstract: Binary tropical cyclones (BTCs) typically refer to the coexistence of two tropical cyclones (TCs) within a specific distance range, often resulting in disastrous rainstorms in coastal areas of China. However, the differences in rainfall and underlying causes between BTC-influenced typhoons and general typhoons remain unclear. In this article, the TC closer to the rainfall center in the BTC is referred to as the target typhoon (tTC), while the other is termed the accompanying typhoon (cmp_TC). This study compares and analyzes the rainfall differences and potential causes of tTCs and similar typhoons (sim_TC) with a comparable track but which are unaffected by BTCs from 1981 to 2020. The results show that: (1) On average, tTCs and cmp_TCs experience 18.79% heavier maximum daily rainfall compared to general TCs, with a significantly increased likelihood of rainfall $\geq$250 mm. (2) Given similar tracks, the average rainfall for tTCs (212.62 mm) is 30.2% heavier than that for sim_TCs (163.30 mm). (3) The analysis of potential impact factors on rainfall (translation speed, intensity, direction change) reveals that sim_TCs move at an average of 21.38 km/h, which is about 19.66% faster than the 17.87 km/h of tTCs, potentially accounting for the observed differences in rainfall. (4) Further investigation into the causes of west–east oriented BTC rainfall in the Northern Fujian (N_Fujian) region suggests that water vapor transport and slowing down of the translation speed are the possible mechanisms of BTC influence. Specifically, 80% of tTCs receive water vapor from the direction of their cmp_TC, and the steering flow for tTC is only 59.88% of that for sim_TC.

Keywords: binary tropical cyclones; similar-track tropical cyclones; extreme precipitation; China

Citation: Wang, M.; Ren, F.; Chen, G.; Lin, X. Rainfall Differences and Possible Causes of Similar-Track Tropical Cyclones Affected and Unaffected by Binary Tropical Cyclones (BTCs) in China. *Remote Sens.* **2024**, *16*, 1692. https://doi.org/10.3390/rs16101692

Academic Editors: Vincenzo Levizzani and Ehsan Sharifi

Received: 17 March 2024
Revised: 8 May 2024
Accepted: 8 May 2024
Published: 9 May 2024

1. Introduction

Tropical cyclones are fierce weather systems with extremely strong destructive power, accounting for 38% of disasters caused by weather, climate and hydrology [1]. China, situated in the Western North Pacific Ocean (WNPO), experiences an average of 7-8 landfalling TCs annually, making it one of the most frequently affected regions [2,3]. With the ongoing effects of global warming, the TC disasters that China faces are on the rise [4,5]. According to statistics reported by Lei et al. (2009) and Lei (2020), the direct economic losses due to TC-induced rainstorms, strong winds and storm surges each year account for about 0.4% of China's GDP, and the casualties are about 9000 people (with more than 500 deaths) [6,7], representing about 13% and 21% of China's meteorological disaster economic and human losses, respectively [8–10]. Therefore, improving the TC rainfall operational forecasting capabilities is of great significance for improving the monitoring and early warning system and enhancing the disaster-resilience capabilities.

Despite steady improvements in predicting TC genesis and tracks, advancements in fine-scale TC rainfall forecasting have been minimal [11–17]. Especially under the influence of BTC, TC forecasts face heightened uncertainty, driven by more erratic movement and complex water vapor exchange [18–25]. The BTC happens when two coexisting TCs are within defined distance thresholds—approximately 12° latitude (Carr et al., 1997, 1998) [26,27], 1600 km (Jang and Chun, 2015) [22], or 1800 km (Ren et al., 2020) [28]—which can influence the TC track, intensity and rainfall patterns. The intricate interplay between the two TCs and the environmental flow field [18,24,29–32], as well as the water vapor transport between the TCs [33,34], makes it difficult to accurately forecast the extreme precipitation events under the BTC influence [25,35–38]. Previous studies mainly focused on BTC impacts on the track [18,19,23] and intensity [29,31] of TCs, analyzing specific cases of extreme rainfall induced by BTCs [34,36–38]. These studies have not addressed critical scientific questions: what are the distinct differences in TC rainfall between those influenced by BTC and normal TCs, and what are the underlying mechanisms contributing to these differences? Addressing these inquiries holds significant importance for providing comprehensive and practical guidance in operational forecasting.

This paper systematically conducts a comparative analysis of rainfall differences and potential causes in similar-track TCs with and without BTC influence. Track is a critical factor determining TC precipitation [39,40], and reflects the characteristics of the underlying topography and large-scale environmental circulations of TCs [41]. Comparing similar-track TCs is a widely adopted method in operational forecasting and scientific analysis [42–45], as they share common features, especially concerning precipitation, providing a theoretical basis for numerous statistic- or analog-based forecast models [46–53]. Thus, this study aims to deepen the understanding of TC rainfall under BTC influence and provide some reference for TC rainfall prediction by conducting a long-term comparative study (1981–2020) of rainfall and potential rainfall influencing factors of tTC and its sim_TC. Subsequent sections describe the data and methodology used in the study, with Section 3 presenting the results of rainfall differences and possible causes for tTC and sim_TC, followed by the summary and concluding remarks in the final section.

2. Data and Methodology

2.1. Data

The TC best-track dataset obtained from the Shanghai Typhoon Institute (STI) of the China Meteorological Administration (CMA) is used in this study. It covers the period from 1981 to 2020 and includes the observed TC locations and intensities over the WNPO at 6 h intervals [54], measured as 2 min mean maximum sustained wind speed (V_{MAX}) and minimum sea-level pressure (P_{MIN}). For TCs situated over open ocean areas, the dataset employs the Dvorak [55] technique on satellite remote sensing data of infrared and visible cloud images to identify critical information about TCs, such as position, intensity, structure, size, and precipitation. Only TCs that reach or exceed the tropical storm level ($V_{MAX} > 17.5$ m/s) are included in this study.

The daily precipitation data observed over the 40-year period are provided by the CMA/National Meteorological Information Center, covering 2027 rain gauge stations across most of China (Figure 1), with 2006 on mainland China and 21 on the island of Taiwan. The daily amounts are defined as those from 1200 UTC to 1200 UTC.

The ERA5 dataset [56], a state-of-the-art product of the European Centre for Medium-range Weather Forecasts (ECMWF), uses advanced four-dimensional variational (4D-Var) assimilation techniques and sophisticated models to integrate a vast array of observations from various sources. Remote sensing instruments, such as ground-based radar and satellite sensors, play a crucial role in this integration. In particular, satellite sensors provide global coverage and high-resolution data that are essential for accurate and reliable weather forecasting. By calibrating and correcting the satellite data with in situ measurements, the ERA5 dataset achieves a high level of robustness and comprehensiveness. In this study this dataset with a grid spacing of 0.25° × 0.25° and 37 vertical layers at 6 h intervals

(i.e., four times per day), including horizontal winds, specific humidity, temperature, and geopotential height, is used to examine the large-scale environments in which the BTCs develop.

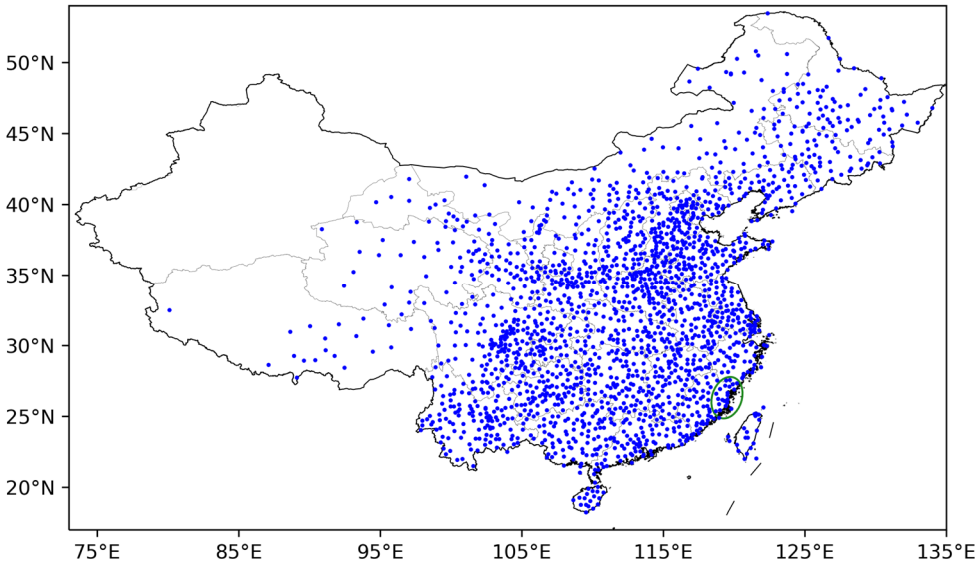

Figure 1. Distribution of the 2027 rain gauge stations in China. The green ellipse highlights the Northern Fujian region.

The GDAS1 dataset is the output of the Global Data Assimilation System (GDAS) developed by the National Centers for Environmental Prediction (NCEP). This system assimilates multi-platform observational data, including satellite and radar data. In the present study, parameters from this dataset such as geopotential height, horizontal winds, temperature, specific humidity, and surface pressure, with a horizontal resolution of 1° × 1° and 21 layers in the vertical direction at 6 h intervals (i.e., 00, 06, 12, and 18 UTC) are used to drive the Hybrid Single-Particle Lagrangian Integrated Trajectory (HYSPLIT) model, which aims to simulate the transport of water vapor and analyze its potential contribution to BTC heavy rainfall events.

To provide a clear overview of the datasets utilized in this study, the main characteristics and sources of the data are summarized in Table 1.

Table 1. Data sources and related information.

Dataset	Period	Grid Resolution	Temporal Resolution	Recourses
TC best-track	1949–present	--	6 h	https://typhoon.slt.zj.gov.cn/default.aspx (accessed on 13 March 2024)
Rain gauge observation	1949–present	2027 station	1 day	https://data.cma.cn/en/ (accessed on 13 March 2024)
ERA5	1940–present	0.25° × 0.25°	1 h	https://www.ecmwf.int/en/forecasts/datasets (accessed on 13 March 2024)
GDAS1	2006–present	1° × 1°	6 h	ftp://arlftp.arlhq.noaa.gov/pub/archives/gdas1 (accessed on 13 March 2024)
This work	1981–2020	--	--	--

2.2. Methodology

2.2.1. Definition of BTC Rainfall

The definition of BTCs in the WNPO, proposed by Ren et al. (2020) [28], considers two coexisting TCs within a distance of 1800 km or less and persisting for a minimum

duration of 12 h. Once BTCs are identified, the Objective Synoptic Analysis Technique (OSAT; Ren et al., 2001, 2007) is used to identify TC precipitation [57,58]. This technique is based on the distance from TC center to the region of precipitation, i.e., the proximity and continuity between neighboring raining stations, in order to trace TC-influenced rain belts that may extend from 500 km to 1100 km away from the TC center. Then, the BTC rainfall can be defined as the inland precipitation produced by one or both TCs in the duration of BTC. A maximum value in a specific day, i.e., the date of the BTC maximum daily rainfall (BTCMRD) at a certain rain gauge station, always exists. This refers to the center of the BTC daily precipitation, namely the BTC maximum daily rainfall, which is our concern in this study. In this way, a list of BTCs producing rainfall in China (or the N_Fujian region) during 1981–2020 can be obtained.

2.2.2. Identify the Similar-Track Normal Typhoon of Target TC

Figure 2 shows the flowchart of obtaining the information of target TC (tTC) and its similar TC (sim_TC). The first step involves identifying the tTC from the BTCs based on the distance between two TCs and the rain gauge station with the BTC maximum daily rainfall. The TC closer to the station is considered the tTC, while the other considered the cmp_TC. Next, we determine a similarity region based on the track and direction of the tTC on the day before, the day of, and the day after the BTCMRD. The similarity region is a rectangular area bounded by the maximum and minimum latitudes and longitudes of the tTC's three-day track. The region is expanded in the direction perpendicular to the orientation of the track. For example, if the track is oriented east–west, the region is widened in the north–south direction; if the track is oriented south–north, the region is widened in the east–west direction.

Subsequently, the third step involves identifying a sim_TC within the similarity region. This sim_TC should be unaffected by BTC during its rainfall process. To identify such a TC, the Track Similarity Index (TSAI) is calculated for the tTC and all historical BTCs unaffected TCs in this similarity region. The TSAI represents an enclosed area bounded by two TC tracks with two lines connecting their initiating and ending points (cf. Figure 1 in Ren et al., 2018 [50]). A smaller TSAI value indicates higher similarity between historical TCs and the tTC. Thus, the TC with the smallest TSAI value is considered the sim_TC of the tTC. Upon identifying sim_TC, the subsequent steps include determining the average location of tTC on the BTCMRD. The time when the sim_TC is closest to this position is obtained, serving as a reference point T. Subsequently, we screen for any daily rainfall of sim_TC within the period between T − 12 h to T + 12 h; the period may span across two different days. The day closest to T is selected as the corresponding rainfall day for sim_TC in relation to the BTCMRD. However, if the distance between the mean position of tTC on the BTCMRD and the mean position of sim_TC on the corresponding rainfall day is $\geq$240 km (which is approximately the mean radius of TCs in the WNPO [59,60]), the samples are discarded. Finally, we gather information about tTC on BTCMRD and sim_TC on the corresponding rainfall day.

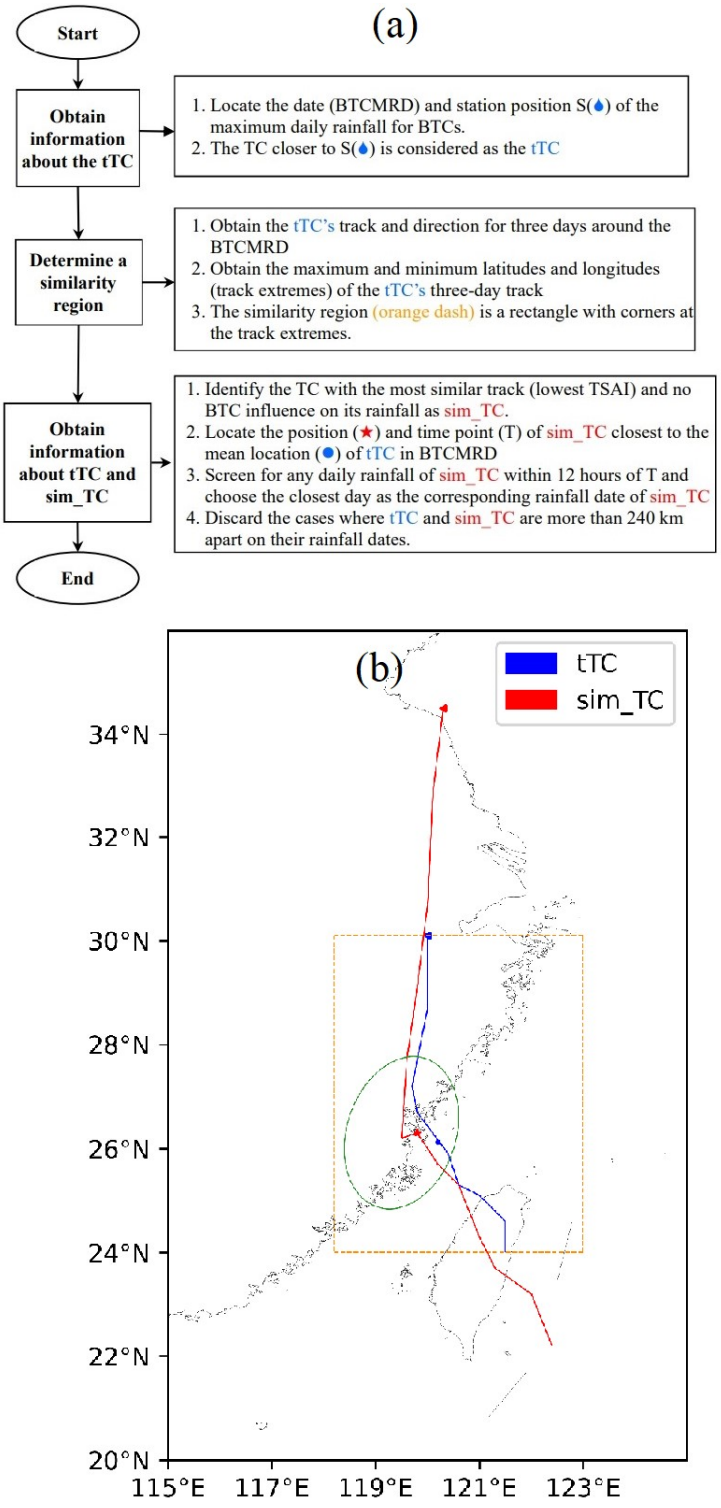

Figure 2. Flowchart (**a**) and example (**b**) of obtaining the information of the target TC (tTC) that caused the primary impact in BTC and its similar-track TC that without BTC influence (sim_TC), where blue represents the tTC (Typhoon Morakot, 2009), red represents the sim_TC (Typhoon Toraji, 2001), green ellipse represents the Northern Fujian region, the raindrop shape represents the location of the BTC's maximum daily rainfall, the blue dot represents the mean position of the tTC on the day of BTCMRD, the red five-pointed star represents the mean position of the sim_TC on the corresponding day of the BTCMRD, and the orange dashed line represents the similarity region.

2.2.3. Diagnosis of Moisture Transport between BTCs

The HYSPLIT model, developed by the National Oceanic and Atmospheric Administration (NOAA) [61], is widely used to generate air mass backward trajectories, which allows users to simultaneously release particles from all points within a specified matrix at a given time and height. In this study, we focus on the moisture sources of the tTC on the day it produced maximum daily rainfall in the Northern Fujian region. To this end, we define a target area as a $6^\circ \times 6^\circ$ square, which encompasses 49 grid points and is centered around the location of the tTC. Then, particles are released at each grid point at an altitude of 1500 m, and the 72 h backward trajectories of these particles are calculated hourly by HYSPLIT, resulting in the generation of 1176 trajectories for each tTC. Next, the trajectories are clustered into groups (hereafter referred to as clusters) with similar transport patterns based on the Total Spatial Variance (TSV) method [62]. For specific steps, please refer to Section 2.3 in (Su et al., 2015 [63]). Subsequently, the distance between each cluster and the track of cmp_TC was calculated. Clusters originating from the direction of cmp_TC and having a minimum distance of $\leq$450 km (roughly corresponding to the mean size of TCs in the WNPO [59,60]) to cmp_TC are considered to indicate a water vapor transport passage for the tTC coming from the direction of cmp_TC. The contribution rate of each cluster is determined by the number of trajectories it contains (since the differences in specific humidity between clusters are negligible in this study, a qualitative assessment suffices for diagnosing moisture transport between two TCs). After all the previous steps, the existence and contribution rate of water vapor transport between BTCs can be determined.

3. Results

3.1. Rainfall Differences and Causes of tTC and Its sim_TC for Nationwide Samples

The fundamental premise of this study is that there is a difference in typhoon rainfall patterns between those influenced by the BTC effect and general typhoons. As depicted in Figure 3a, the mean and median of the maximum daily rainfall for BTC-affected cases (comprising both tTC and cmp_TC) were 233.96 mm and 201.4 mm, respectively, which surpassed those of the general TC cases (196.96 mm and 174.75 mm). The probability distribution histograms for both groups illustrate the distribution of rainfall across various intervals, following a parabolic shape and peaking in the heavy rain interval (100–250 mm). Notably, the probability of BTC-influenced TCs producing maximum daily rainfall exceeding 100 mm was 13.05% higher than that of general TCs (79.59% vs. 70.40%). As the extremity of rainfall increased, the disparities in the occurrence rates of strong precipitation between the two groups became more pronounced. As illustrated in Figure 3b, the probability distribution histograms for maximum process rainfall in both BTC-influenced and unaffected cases exhibit similar characteristics to those observed in maximum daily rainfall. The mean and median values of maximum process rainfall influenced by the BTC effect were 345.84 mm and 268.65 mm, respectively, surpassing the values for cases unaffected by the BTC, which were 271.84 mm and 215.80 mm, respectively.

These observations were further supported by statistical analysis. Specifically, a one-tailed two-sample *t*-test was conducted at a significance level of $\alpha = 0.01$ to test for a statistically significant impact of the BTC effect on rainfall, with the expectation that the mean daily (process) maximum rainfall for BTC-affected TCs (tTC and cmp_TC) would be greater than that for general (BTC-unaffected) TCs. The results indicated statistically significant differences ($p < \alpha$), supporting our expectation that BTC-affected TCs exhibit higher maximum daily (process) rainfall compared to general TCs.

The above findings suggest that the BTC effect significantly influences typhoon precipitation, leading to heavier rainfall and increased probabilities of rainfall extremes. Further investigation is needed to understand the mechanism through which the BTC effect influences typhoon rainfall.

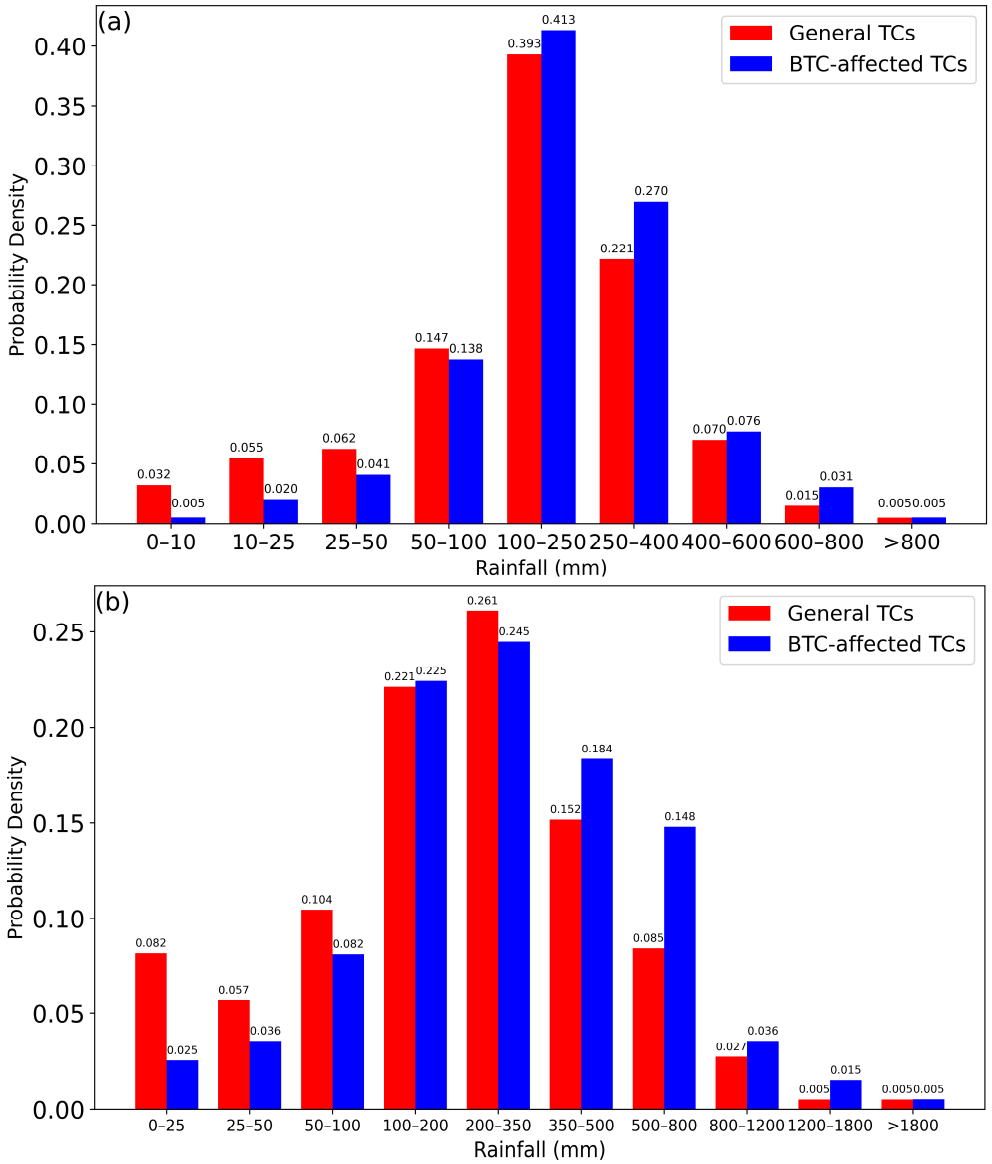

Figure 3. Probability density histogram of TCs affected (BTC-affected) and unaffected (General) by the binary tropical cyclones effect from 1981 to 2020: (**a**) maximum daily rainfall, (**b**) maximum process rainfall.

Since the track of TC reflects, to some extent, the large-scale circulations and underlying topography where the TC situated [39,41], the target TC and its historical analogs share similar topography and large-scale circulation systems that jointly influence precipitation. Hence, to emphasize the BTC effect more distinctly, we compare similar-track TCs with and without the BTC influence. As described in Section 2.2.2, we obtained the rainfall, translation speed, intensity, and other information of 94 pairs of tTC and sim_TC from 1981 to 2020. This study focuses on the differences in rainfall and rainfall influencing factors between tTC on the date of the BTC maximum daily rainfall (BTCMRD) and sim_TC on the corresponding rainfall day. Therefore, unless otherwise specified, the rainfall and rainfall influencing factors of tTC and its sim_TC mentioned in the following text all refer to this period.

The rainfall differences between tTC and sim_TC are illustrated in Figure 4. The rainfall of tTC was heavier than that of sim_TC, with the mean and median values of 212.63 mm and 189.55 mm, respectively, compared to 171.37 mm and 159.05 mm for sim_TC. The results of the one-tailed two-sample *t*-test, conducted with the expectation that the maximum daily

rainfall for tTCs would be greater than that for sim_TCs, confirm ($p < 0.01$) the significant contribution of the BTC effect to heavier rainfall. Figure 4a also shows the probability of tTC experiencing heavy rainfall (≥50 mm) was 13.5% higher than that of sim_TC, and as the rainfall extremity increased, the difference in the occurrence rate of rainfall between tTC and sim_TC became more pronounced. In other words, under the influence of the BTC effect, TC precipitation was not only heavier, but also more likely to result in extreme rainfall events. The rainfall differences between individual cases of tTC and sim_TC are illustrated in Figure 4b. When the rainfall of tTC was <300 mm, the corresponding rainfall of sim_TC fluctuated around it, and in some cases, the two were nearly identical. However, when the rainfall of tTC was ≥300.00 mm, the corresponding rainfall of sim_TC was always lower than that of tTC. Additionally, tTC had six occurrences of extreme rainfall (exceeding 475 mm), which was beyond the reach of sim_TC. These results indicate that, under the constraint of similar underlying topography and environmental conditions, the TC rainfall influenced by the BTC effect was generally heavier and had a higher probability of producing extreme heavy rainfall.

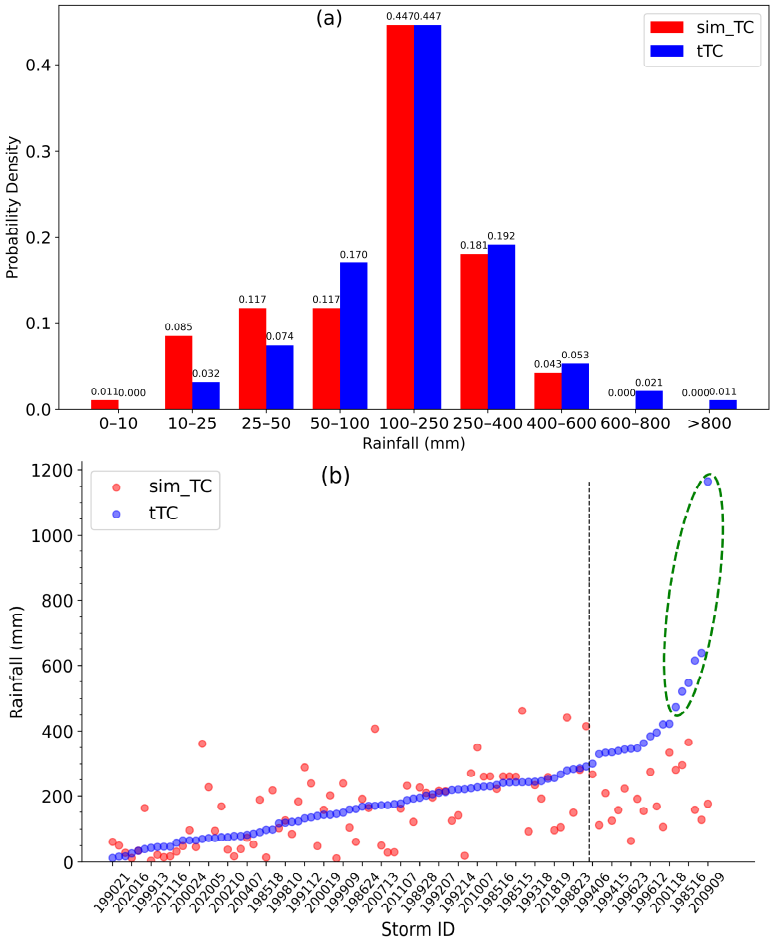

Figure 4. Rainfall differences between the target TC (tTC) and its similar TC (sim_TC) from 1981 to 2020: (**a**) probability distribution, (**b**) individual sample magnitude (units: mm), sorted in ascending order of tTC rainfall. (n = 94).

Factors such as translation speed and intensity have a significant impact on TC precipitation [39,64,65]. Moreover, many studies have shown that the BTC effect causes the track of TCs to change irregularly and suddenly [23,26,27,29,32]. Therefore, we consider the translation speed ($V = \text{distance}(P_{t+1} - P_{t-1})/2t$, where P_{t-1} and P_{t+1} represent the TC positions at the previous and next time steps, respectively), intensity, and direction change ($\Delta\theta = \text{abs}(\theta_t - \theta_{t-1})$, where $\theta_t = \text{direction}(P_t - P_{t-1})$, $\theta_t = 0°, 90°, 180°, 270°$ represent TC

moving eastward, northward, westward, and southward, respectively) as factors that may influence typhoon precipitation for diagnostic analysis.

Figure 5a shows distinct differences in the translation speed of tTC and sim_TC. The Probability Density Function (PDF) estimate curve of tTC's translation speed roughly follows a parabolic distribution, peaking at around 15.5 km/h with a probability density at the peak falling within the range of 0.3 to 0.35. The mean and median of the translation speed were 17.87 km/h and 16.78 km/h, respectively. In contrast, the PDF curve of sim_TC's translation speed is also unimodal, with the peak around 19 km/h and the probability density at the peak over 0.4, indicating that sim_TC's translation speed was more concentrated around 19 km/h. The mean and median of the translation speed were 21.38 km/h and 19.71 km/h, respectively, both faster than tTC's. The one-tailed two-sample *t*-test was conducted to evaluate the mean translation speed difference, with the expectation that sim_TC would move faster than tTC. The results, significant at the 99% confidence level, support this expectation, indicating that sim_TC indeed translates at a higher speed compared to tTC. Figure 6 helps illustrate a statistically significant weak negative correlation between tTC's translation speed and precipitation ($R = -0.284$, $p < 0.01$), indicating that this relationship is unlikely to have occurred by chance. This correlation may suggest that slower-moving TCs are more likely to result in sustained heavy precipitation in specific regions, which aligns with the well-established consensus in meteorological research [64,66]. Sim_TC has a 19.66% faster translation speed, which possibly contributes to the smaller precipitation compared to tTC. However, the low correlation coefficient and the deviations between the fitting line and the data points indicate the intricate mechanisms underlying TC rainfall. TC rainfall is influenced by various factors, including translation speed, moisture supply, the typhoon's internal structure, the presence of strong upward motion, and local terrain, among others.

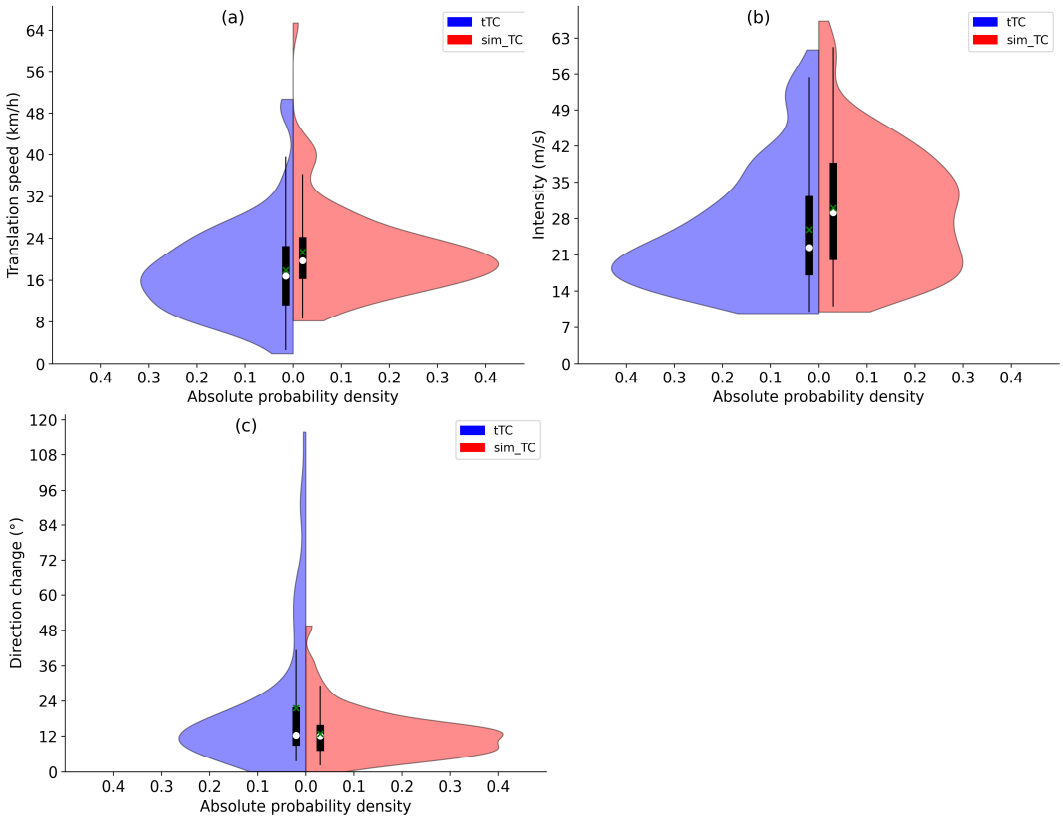

Figure 5. Probability Density Function (PDF) estimate plot of rainfall potential influencing factors of tTC and sim_TC from 1981 to 2020: (**a**) translation speed, (**b**) intensity, and (**c**) direction change. ($n = 94$, the white dots represent the median, and the green "x" represents the mean).

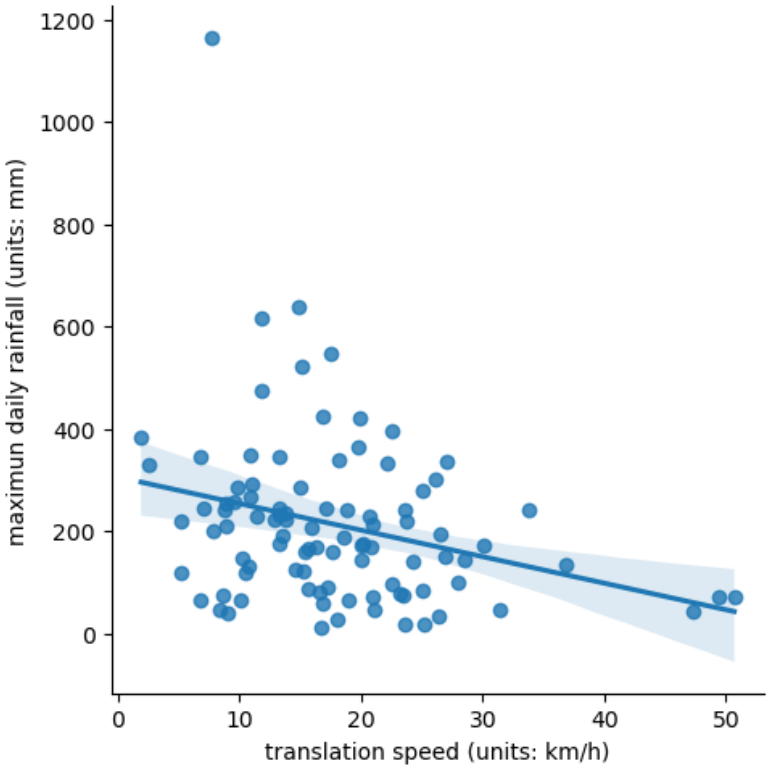

Figure 6. Scatter plots and linear regression fits between maximum rainfall and translation speed of tTC during the date of BTC maximum rainfall from 1981 to 2020. (n = 94; shaded areas indicate the 95% confidence intervals around the fitted lines).

As depicted in Figure 5b, notable differences in intensity between tTC and sim_TC are evident. The mean and median intensity for tTC were 25.8 m/s and 22.375 m/s, respectively. Its PDF curve follows a unimodal distribution, peaking around 18.5 m/s with a probability density at the peak falling in the range of 0.4 to 0.45, indicating that tTC's intensity was more concentrated around 18.5 m/s. In contrast, the PDF curve of sim_TC's intensity exhibits a bimodal distribution, with the primary peak around 19.5 m/s and a secondary peak around 33.0 m/s, suggesting a more dispersed distribution of sim_TC intensities. The mean and median of sim_TC's intensity were 30.02 m/s and 29.125 m/s, respectively, both higher than those of tTC's. The *t*-test for the mean intensity difference between tTC and sim_TC indicates that sim_TC is stronger than tTC, and this difference is significant at the 99% confidence level. A Pearson correlation test shows a positive correlation between tTC's intensity and its rainfall, with a correlation coefficient of 0.171. However, this correlation fails to pass the significance test ($p = 0.099$). Therefore, we can only cautiously assume that stronger typhoons may be somewhat associated with more extreme precipitation events.

In terms of direction change (Figure 5c), the median values of tTC and sim_TC are almost identical, both around 12°, but tTC's direction change has much higher dispersion than sim_TC's. Under the premise of similar tracks, tTC, influenced by the BTC effect, exhibits greater uncertainty in the movement direction, potentially leading to 90° turns and spinning. The correlation test shows that tTC's direction change has no obvious relationship with its rainfall. However, the negative correlation between tTC's direction change and translation speed ($R = -0.423$, $p < 0.01$) indicates that larger direction changes may contribute to more erratic or spinning movements, subsequently leading to slower translation speeds (figure omitted). Slower-moving TCs are more likely to produce greater precipitation. Therefore, if the typhoon track involves turning and lingering, it may indirectly lead to large rainfall.

The findings above indicate that tTCs exhibit statistically significantly heavier rainfall compared to their similar-track counterparts, which can be partially attributed to the slower translation speed of tTCs, leading to increased precipitation accumulation.

3.2. Rainfall Differences and Causes of tTC and Its sim_TC for the Northern Fujian Region Samples

Due to the extensive coastline in China, the primary influencing factors on TC rainfall may vary across different regions [41,67]. As pointed out by Wang et al. (2020), extreme rainfall associated with the BTC effect in China is prominent in three typical regions—the Pearl River Delta, Northern Fujian Province, and Taiwan Island [33]. Therefore, a thorough investigation into the impact of the BTC effect on precipitation requires focus on a specific area. This study, limited by space, concentrates on 32 BTC samples that influenced the Northern Fujian (N_Fujian) region from 1981 to 2020 to explore the causes of BTC-associated heavy rainfall in this representative region.

As depicted in Figure 7, the mean and median of tTC precipitation in the N_Fujian region are 164.97 mm and 153.8 mm, respectively, whereas those of sim_TC are 97.35 mm and 68.9 mm, respectively, both of which are lower than tTC. A paired sample Student's *t*-test revealed statistically significant a mean difference between the two at the 99% confidence level. In summary, tTC exhibits a heavier precipitation pattern than sim_TC, with a higher probability of producing extremely heavy precipitation in the N_Fujian region.

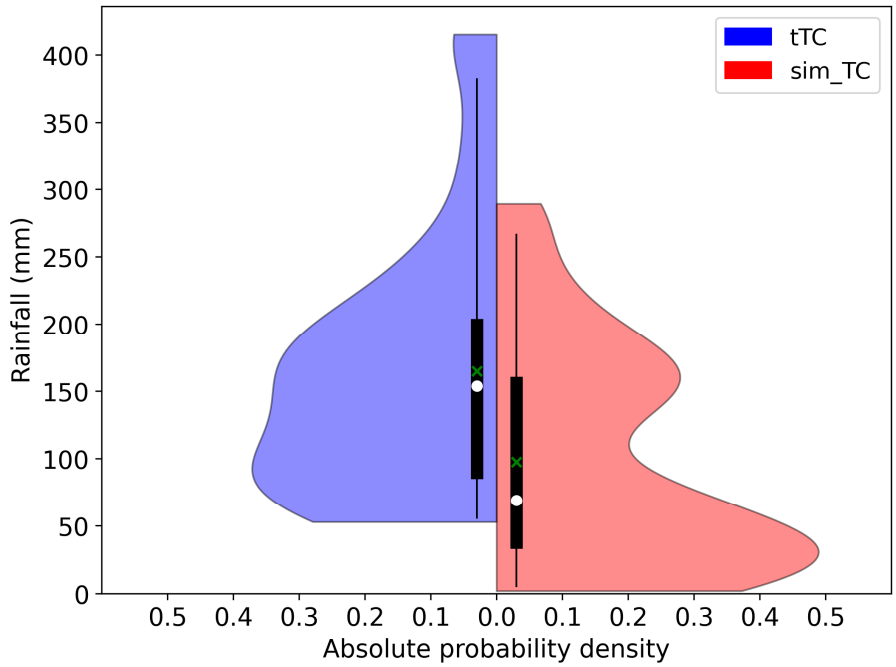

Figure 7. As Figure 5, but for the precipitation (units: mm) of tTC and sim_TC in the Northern Fujian (N_Fujian) region from 1981 to 2020 (n = 32).

In the diagnostic analysis, BTC rainfall cases in the N_Fujian region, similar to the national-scale samples, translation speed, intensity, and direction change were selected as potential factors influencing typhoon precipitation. From the perspective of translation speed (Figure 8a), significant differences are observed between the tTC and the sim_TC in the N_Fujian region. The PDF curve of tTC's translation speed roughly follows a unimodal distribution, peaking at around 12 km/h with a probability density at the peak falling in the range of 0.4, to 0.45. The mean and median translation speeds for tTC are 17.78 km/h and 15.75 km/h, respectively. Conversely, the PDF curve of sim_TC's translation speed exhibits a bimodal distribution, with the primary peak around 17.5 km/h and a secondary peak around 27.5 km/h, and the probability density of both peak is slightly larger than

0.4, suggesting that sim_TC's translation speed is more concentrated around these values. The average translation speed of sim_TC is 22.53 km/h, which is 39.59% faster than that of tTC, and the mean translation speed difference is statistically significant at the 95% confidence level. This marked difference in movement may be a key factor contributing to the significant differences in precipitation between tTC and sim_TC.

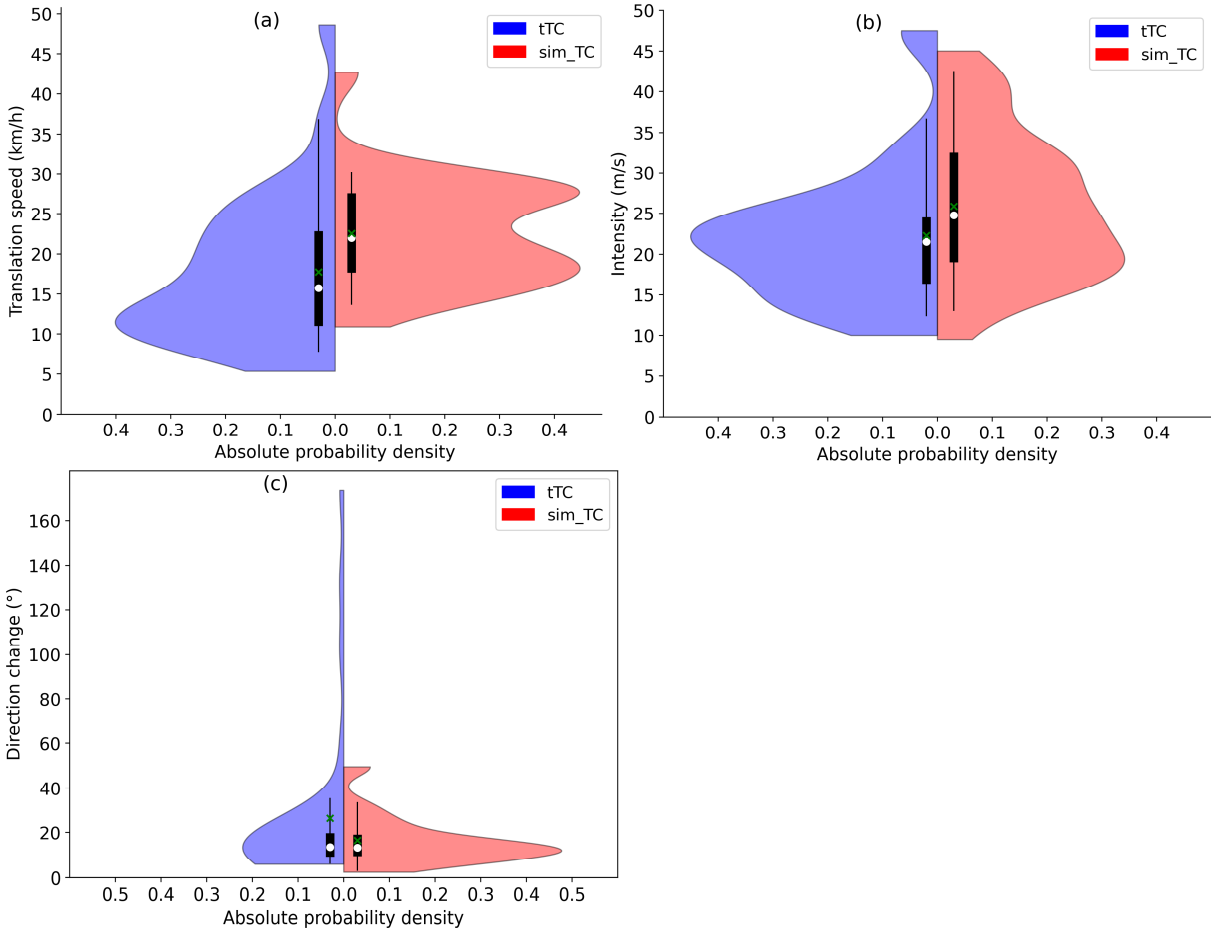

Figure 8. As Figure 5, but in the Northern Fujian (N_Fujian) region (n = 32).

In terms of intensity (Figure 8b), the mean and median of tTC's intensity in the N_Fujian region are 22.26 m/s and 21.50 m/s, respectively. The PDF curve of tTC's intensity displays a roughly unimodal distribution, peaking at 23.0 m/s, with the probability density at peak falling in the range of 0.45 to 0.5, indicating that tTC's intensity is more concentrated around 23.0 m/s. In contrast, the PDF curve of sim_TC's intensity also shows a unimodal distribution, but its peak is around 19.0 m/s, and the probability density at peak falling in the range of 0.3 to 0.35, suggesting that sim_TC's intensity is more dispersed. The average and median intensity of sim_TC are 25.88 m/s and 24.75 m/s, respectively, both stronger than those of tTC. Despite the higher mean and median intensities of sim_TC compared to tTC, the intensity difference did not reach statistical significance.

Regarding the direction change (Figure 8c), the mean and median direction change of tTC in the N_Fujian region are 26.34° and 13.30°, respectively, while those of sim_TC are 16.35° and 13.09°, respectively. The PDF curves indicate that tTC's direction change is relatively unstable with high dispersion, and there is a possibility of abrupt changes in the track, such as reverse movement ($\Delta\theta \approx 180°$) or right-angle turn ($\Delta\theta \approx 90°$), whereas sim_TC's direction change is more concentrated around the peak ($\Delta\theta \approx 13°$), with a peak probability density ≈ 0.5, and a smaller variance. The difference in track deflection angle

between tTC and sim_TC may explain the notable difference in translation speed between the two, subsequently accounting for their pronounced difference in precipitation.

The results indicate that in the N_Fujian region, tTC exhibits lower intensity compared to sim_TC. However, tTC's precipitation is heavier than that of sim_TC. This difference may be partly attributed to the BTC effect, which leads to the erratic movement and slower translation speed of tTC, contributing to increased precipitation.

Beyond intrinsic factors such as translation speed, intensity, and direction change, environmental factors like water vapor also play a crucial role in influencing the development and maintenance of TCs [40,68], thereby impacting typhoon rainfall. In both research and practical applications, the analysis of water vapor often focuses on lower atmospheric levels, particularly at 850 hPa. In this study, particles were released at an altitude of 1500 m above sea level, corresponding to 850 hPa level. A backward 72 h water vapor tracing was conducted to identify the sources of water vapor for tTC on the day it produced maximum daily rainfall in the N_Fujian region (details provided in Section 2.2.3). Due to data limitations (as GDAS1 data are available from 2006 onward), only 15 tTCs that impacted the N_Fujian region between 2006 and 2020 were traced.

As shown in Table 2, 80% of the samples exhibit water vapor sources originating from the direction of the accompanying typhoon (cmp_TC) in the BTC. These water vapor sources accounted for 6% to 73% of the total water vapor sources of tTC. The three tTCs without water vapor transport from the cmp_TC had relatively small precipitation amounts, ranking (15/15), (11/15), and (9/15), and much lower than the overall mean (175.37 mm). This implies a high likelihood of water vapor transport between BTCs, and these water vapor transport passages play a crucial role in the occurrence of extreme typhoon precipitation in the N_Fujian region.

Table 2. Tracing results of water vapor sources for tTC on the day of maximum daily rainfall in the Northern Fujian (N_Fujian) region.

tTC	cmp_TC	Maximum Rainfall on N_Fujian (Units: mm)	Distance [1] (Units: km)	Total Clusters	Cluster Number [2]	Accounting [3] (Units: %)
200610	200611	212.5	77.1	3	3	34
200909	200908	415.2	412; 175.3	4	1; 4	38; 14
200909	200910	415.2	200.2	4	3	29
201007	201008	66.7	364.9	6	6	6
201009	201007	66.7	16.4; 24.2	5	1;4	21;20
201009	201008	66.7	374.0; 32.8	5	3;6	34; 6
201205	201206	99.5	450>	3	/	/
201210	201211	189.9	40.3; 23.7	3	1; 3	39; 34
201210	201212	170	23.8; 105.4	3	1; 3	44; 29
201325	201326	221.4	69.5	3	3	16
201616	201618	251.1	286.2	4	1	23
201711	201710	174.1	43.8	3	2	18
201819	201817	103.3	54.2; 350.1	6	2; 3	15; 37
201821	201817	55	450>	4	/	/
201821	201819	123.2	450>	3	/	/

[1] "Distance": The minimum distance between the cluster and cmp_TC track. A distance greater than 450 km indicates no water vapor transport from cmp_TC, and the 'Cluster number' and 'Accounting' columns will be denoted by '/'. [2] "Cluster number": As described in Section 2.2.3, tTC's water vapor source trajectories are grouped into clusters, each denoted by a unique "Cluster number" automatically assigned by HYSPLIT model. The fifth table column shows "Cluster numbers" within 450 km of the cmp_TC's track. [3] "Accounting" refers to the water vapor contribution rate of each cluster listed in the fifth table column.

The comparative analysis of rainfall impact factors and the results of tracing water vapor sources suggest that the BTC effect may create favorable conditions for more intense precipitation in the N_Fujian region by slowing down tTC's movement and transporting water vapor to tTC. However, further validation of these findings requires a more thorough

diagnostic examination of the surrounding environmental circulations of tTC during heavy rainfall events.

To comprehensively diagnose whether BTC water vapor transport is one of the reasons for the increased likelihood of heavy rainfall in the N_Fujian region, the study conducted a dynamic composite analysis [69,70] for tTCs. Despite restricting the study area to the N_Fujian region, there is still a considerable difference in the relative positions of the two TCs that constitute the BTC (such as their east–west or north–south orientation), and the effects of different orientations of the BTC may be different [37,71]. Therefore, this study further selected eight samples with relatively consistent positions of tTC and its cmp_TC on the BTCMRD for dynamic composite analysis centered on tTC. Aiming to delve deeper into understanding the potential impacts of BTC effect on precipitation.

It is worth mentioning that this subsection primarily analyzes the contribution of BTC to the extreme rainfall in the target region (N_Fujian) on the BTCMRD. Given that the movement distance of tTC and sim_TC within a day is limited, and the selected BTC samples are all east–west oriented with relatively consistent positions of tTC (within 2.0 latitudes from the mean position), the longitude and latitude coordinates were reallocated after the dynamic composite, centering on the mean position of tTC/sim_TC.

The majority of water vapor is present in the lower and middle atmosphere below 300 hPa, and the degree of water vapor transport and convergence determines the distribution of water condensate in clouds and the amount of precipitation [72,73]. As illustrated in Figure 9, the overall water vapor flux field shows that both tTC and sim_TC receive ample water vapor from the low latitudes of the Indian Ocean, carried by the southwesterly monsoonal airstream. However, the South China Sea summer monsoon index (calculated following the method proposed by Dai et al. in 2000 [74]) suggests a stronger southwesterly monsoonal airstream for tTC compared to sim_TC, indicated by a monsoon index of 11.47 for tTC and 10.03 for sim_TC. This implies that the southwesterly monsoonal airstream may contribute more favorably to moisture conditions for tTCs' maintenance and development, resulting in heavier precipitation over the N_Fujian region. This differential monsoonal impact may partly explain the greater rainfall for tTCs compared to sim_TCs.

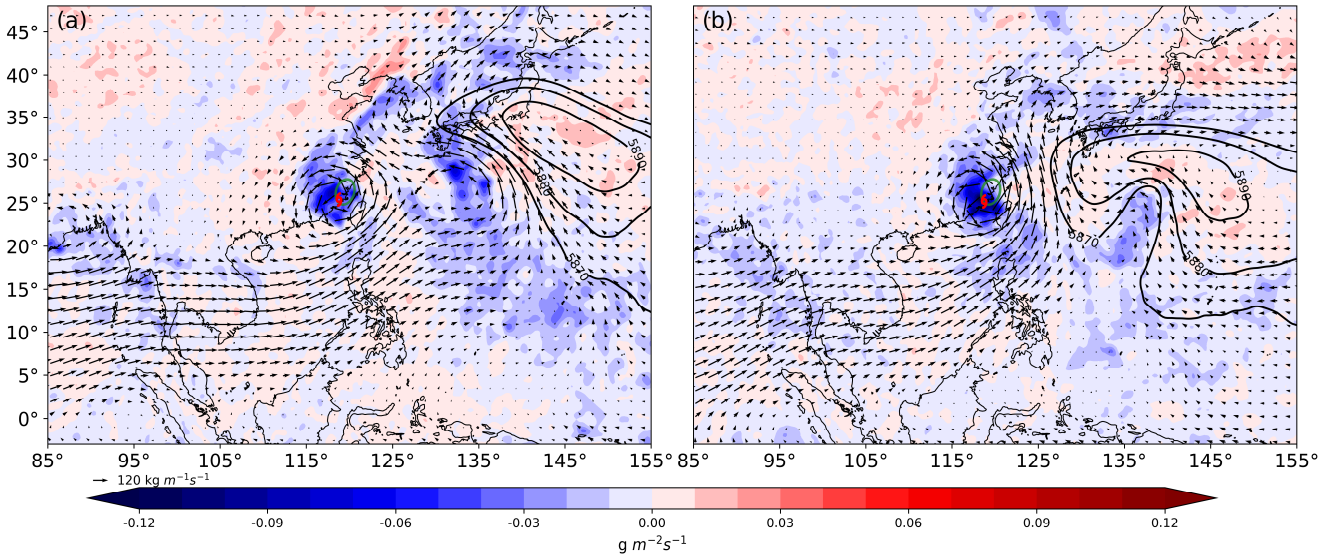

Figure 9. Dynamic composites showing the 1000–300 hPa water vapor flux vectors (arrows) and flux convergence (shadings) for (**a**) tTC (30 time step samples, corresponding to 02:00, 08:00, 14:00, and 20:00 BJT on 21 August 1990; 19 August 1991; 7 August 1996; 9 July 2002; 9 August 2009; 31 August 2010; 4 August 2012; and 7 October 2013) and (**b**) sim_TC (32 time step samples, corresponding to the same four time points on 25 July 2006; 26 August 2004; 18 May 2006; 8 June 1995; 31 July 2001; 25 August 2004; 15 July 2006; and 11 July 2018) on the day of maximum daily rainfall. Black contours denote the 500 hPa subtropical high; ellipses outline the N_Fujian region.

Comparing tTC to sim_TC, the Western North Pacific subtropical high (WNPSH) associated with tTC exhibits slightly weaker intensity and is displaced to a more northerly and easterly position. tTC's cmp_TC is positioned approximately 1300 km to its east, situated to the southwest of the WNPSH. The strong pressure gradient between cmp_TC and the WNPSH stimulates a robust westward flow or low-level jet [75–77]. This environmental field configuration causes cmp_TC to intercept a portion of the southwest water vapor transport channel that would otherwise continue toward the Bohai Bay and the Korean Peninsula. Additionally, cmp_TC gathers water vapor and energy on the south side of the WNPSH, transporting them towards tTC through this westward flow. In contrast, the WNPSH influenced sim_TC is relatively stronger and located on the east of sim_TC. Without an accompanying typhoon, there is only an easterly wave at the corresponding position, which is almost embedded in the south side of the WNPSH. This configuration strengthens the northward flow between the sim_TC and the WNPSH, accelerating the southwesterly water vapor transport northward to the mid-high latitudes, which is unfavorable for water vapor convergence in the region affected by sim_TC.

From the perspective of water vapor flux divergence, both tTC and sim_TC exhibit strong convergence covering the N_Fujian region. However, sim_TC appears to have stronger eyewall convection, but the intense northward flow on its east side prevents the convergence zone from covering the northeastern part of N_Fujian. Regardless of tTC or sim_TC, the overall picture is that the N_Fujian region is covered by the eyewall circulation of the typhoon, resulting in strong moisture convergence in this region. However, due to the stronger average intensity (24.9 m/s) of sim_TC compared to tTC (19.43 m/s), the water vapor convergence in the N_Fujian region under sim_TC's influence is stronger, which is more favorable for the occurrence of heavy rainfall.

To further diagnose the differences in moisture conditions between the tTC and the sim_TC, an examination of the specific humidity field (Figure 10) reveals a significant distinction. In the specific humidity field, cmp_TC to the east of tTC acts as an upstream reservoir, collecting abundant energy fluxes from the surrounding ocean surface through the air–sea interaction. This reservoir effect, coupled with the robust westward airflow generated by the joint influence of cmp_TC and the subtropical high, continuously transports water vapor and energy into the tTC. In combination with Figure 9, the N_Fujian region under the influence of tTC appears more humid, with a sustained water vapor transport between BTCs. This continuous transport establishes favorable conditions for heavy rainfall occurrence in this region, contributing to the reason why, despite exhibiting weaker water vapor flux convergence and TC intensity (19.43 m/s vs. 24.91 m/s) compared to sim_TC, tTC displays stronger precipitation. Additionally, the steering flow (which is defined by the average of winds inside an annulus between 300 and 700 km from TC center from 700 to 300 hPa [78,79], following Chien and Kuo 2011; Chien, 2014) that dominates the movement of the typhoon was also compared. Evidently, tTC's steering flow (1.97 m/s) is significantly lower than that of sim_TC (3.39 m/s), explaining tTC's slower movement (12.72 km/h compared to sim_TC's 23.33 km/h). The smaller steering flow and the slower movement further create favorable conditions for the accumulation of tTC's heavy rainfall in the N_Fujian region.

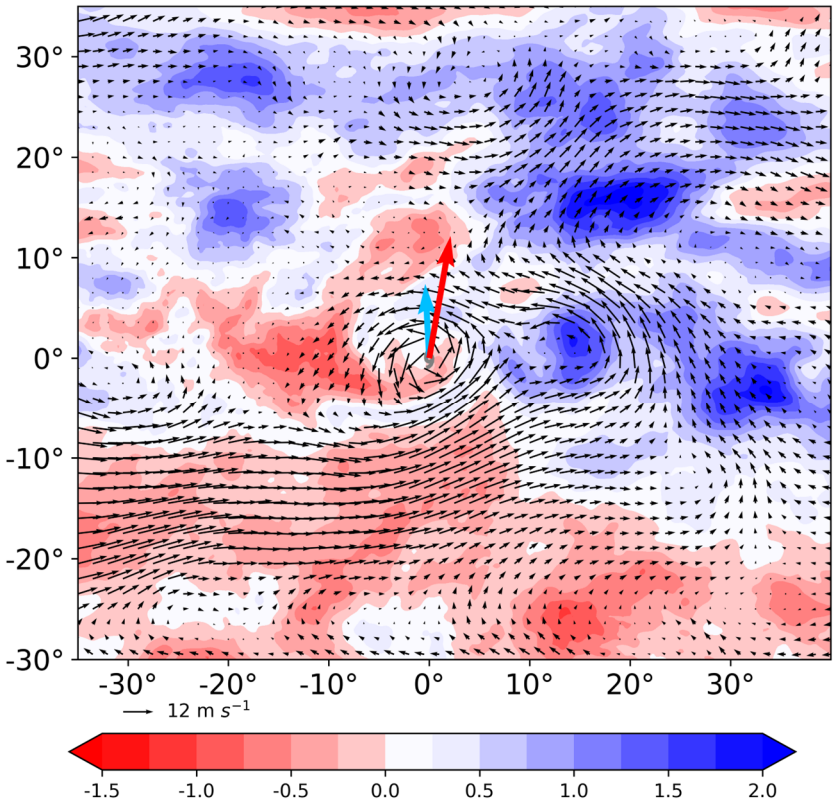

Figure 10. As Figure 9, but for the specific humidity difference (tTC-sim_TC) (shadings, units: g/kg) and the wind field at 850 hPa for tTC (vectors). The blue elongated arrow indicates the average steering flow for tTC and the red elongated arrow indicates the average steering flow for sim_TC.

Based on the analysis above, we can conclude the mechanism of BTC producing extreme rainfall in the N_Fujian region for those east–west oriented BTCs. The manifestation of the BTC effect in this configuration is evident in two aspects. Firstly, the cmp_TC on the east side of tTC and the subtropical high collaborate, intercepting a portion of the southwesterly water vapor flux transport and gathering the energy fluxes from the surrounding ocean surface, acting like a reservoir upstream, continuously supplying water vapor to tTC, establishing favorable water vapor conditions for precipitation. Secondly, the BTC effect changes the steering flow of tTC, resulting in a sluggish movement, further facilitating the accumulation of heavy rainfall in the N_Fujian region. Additionally, the presence of the N_Fujian region, situated in the onshore wind direction of tTC and complemented by local elevated hilly terrain, enhances upward motion and convergence of the warm and wet air. These combined factors contribute to the extremely intense precipitation in the N_Fujian region under the influence of tTC (Figure 11).

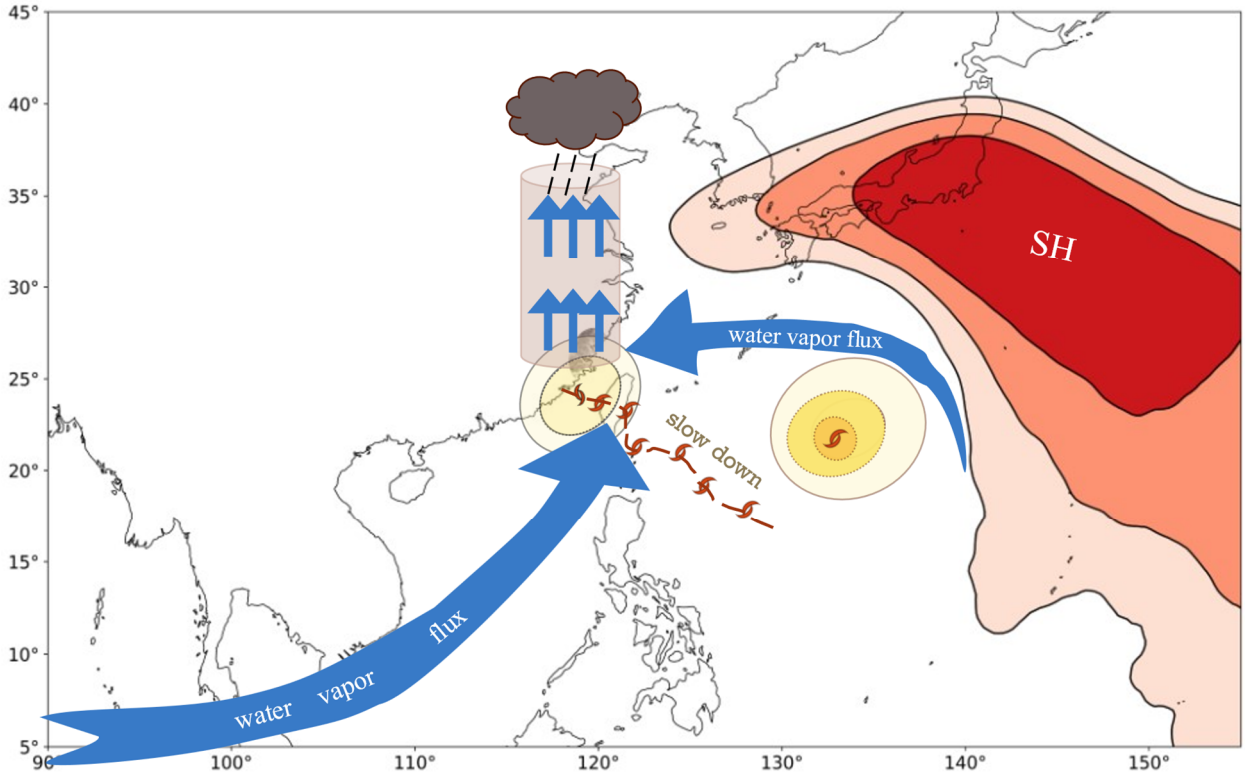

Figure 11. Conceptual model of the extreme rainfall events in the Northern Fujian region under the influence of east–west oriented binary tropical cyclones. 'SH' denotes the Western North Pacific Subtropical High, and the two typhoon symbols represent tTC (typhoon on the west side) and cmp_TC (typhoon on the east side), respectively. Thick blue arrows indicate water vapor flux, upward arrows represent upward motion, and the shaded topography denotes the N_Fujian region.

4. Summary and Concluding Remarks

A statistical comparison analysis of the TC rainfall difference and possible causes between similar-track TCs, whether under the influence of the BTC or not, during the 40-year period of 1981–2020 on the coastal regions of China, was conducted to initially diagnose the effect of the BTC on precipitation. Subsequently, a more in-depth diagnosis and analysis of the mechanisms behind extreme rainfall affected by the BTC were conducted, with a focus on the Northern Fujian (N_Fujian) as the representative high-impact region of BTC-induced rainfall. The key findings are summarized as follows:

(1) The target typhoon (tTC), influenced by the BTC, exhibits significantly greater rainfall compared to the similar-track normal typhoon (sim_TC) (212.63 mm vs. 171.37 mm). Moreover, tTC shows a notably higher likelihood of extreme rainfall, with a 99.77% increased probability of rainfall exceeding 400 mm.

(2) tTC, impacted by the BTC effect, moves in a complex and variable way, resulting in a slow translation speed. This sluggish movement may contribute to heavier rainfall than sim_TC, even when its intensity is lower than sim_TC. These effects consistently influence the rainfall patterns of tTC nationwide, including the N_Fujian region.

(3) Most of the tTCs that influenced the N_Fujian region have water vapor sources from the direction of their accompanying typhoons; the water vapor transport between the BTCs is a possible factor contributing to tTC's intensified rainfall. The mechanism of east–west oriented BTCs producing extreme rainfall in the N_Fujian region is evident in two aspects. Firstly, the strong pressure gradient between cmp_TC and the WNPSH stimulates a robust westward flow, acting like a reservoir upstream and continuously supplying water vapor to tTC. This water vapor is sourced from cmp_TC intercepting southwesterly water vapor flux transport and collecting energy fluxes

from the surrounding ocean surface. Secondly, the BTC effect changes the steering flow of tTC, resulting in a sluggish movement, which facilitates the accumulation of heavy rainfall in the N_Fujian region. Additionally, the N_Fujian region, located in the onshore wind direction of tTC and with local hilly terrain, enhances the upward motion and convergence of the warm and wet air. These factors lead to the extremely intense precipitation in the N_Fujian region under the influence of tTC.

Our study deepens the understanding of TC rainfall under the influence of BTC and reveals that water vapor transport and slowing down the movement are likely the two main ways for BTC effect contributing to intensified rainfall. However, it is crucial to acknowledge that our study relies on some approximations and idealized assumptions, yielding qualitative analytical results. Furthermore, some of our insights were derived from studies conducted in the Fujian region. Their broader application requires empirical validation in diverse regions. Therefore, to thoroughly validate the impact mechanisms of the BTC effect on precipitation, further investigation requires the selection of representative cases. Utilizing numerical models will facilitate the quantitative verification of the BTC effect, particularly in assessing its influence on TC rainfall by changing translation speed and water vapor transport. This additional step is essential for refining and confirming our findings, ensuring a more robust and comprehensive understanding of the intricate dynamics associated with the BTC influence on typhoon-induced precipitation. Moreover, our study exclusively focuses on the onshore precipitation center of typhoons, constraining the exploration of the spatial distribution of precipitation under the BTC effect. To achieve a more comprehensive understanding of BTC effects on rainfall, further research is imperative, incorporating high-resolution observational data, including satellite and radar data, to cover a broader spatial range encompassing both land and ocean areas.

Author Contributions: Conceptualization, M.W. and F.R.; methodology, M.W.; software, M.W.; validation, G.C. and X.L.; writing—original draft preparation, M.W.; writing—review and editing, M.W.; visualization, M.W.; supervision, F.R. and G.C.; project administration, F.R.; funding acquisition, F.R. All authors have read and agreed to the published version of the manuscript.

Funding: This study was supported by the National Natural Scientific Foundation of China (42275037), the Basic Research Fund of CAMS (2023Z016), the Key Laboratory of South China Sea Meteorological Disaster Prevention and Mitigation of Hainan Province (SCSF202307), the Fujian Provincial Department of Science and Technology (2021J01456) and the Jiangsu Collaborative Innovation Center for Climate Change.

Data Availability Statement: Publicly available datasets were analyzed in this study. The best-track data is obtained from http://tcdata.typhoon.org.cn (accessed on 13 March 2024). The precipitation product is downloaded from http://data.cma.cn/ (accessed on 13 March 2024). ERA5 data can be downloaded upon registration through the Climate Data Store (https://cds.climate.copernicus.eu/ (accessed on 13 March 2024)).

Conflicts of Interest: The authors declare no conflicts of interest.

References

1. WMO. *Atlas of Mortality and Economic Losses from Weather, Climate and Water Extremes (1970–2019); WMO: Geneva, Switzerland, 2021.*
2. Chen, L.; Meng, Z. An Overview on Tropical Cyclone Research Progress in China during the Past Ten Years. *Chin. J. Atmos. Sci.* **2001**, *25*, 420–432. (In Chinese)
3. Li, Z.; Zhang, L.; Qian, Q.; Ma, S.; Xu, J.; Dai, K.; Chen, Y.; Wang, Y. The development and consideration of typhoon forecast operation of National Meteorological Center. *Trans. Atmos. Sci.* **2020**, *43*, 10–19. (In Chinese) [CrossRef]
4. Duan, Y.; Chen, L.; Xu, Y.; Qian, C. The status and suggestions of the improvement in the typhoon observation, forecasting and warning systems in China. *Strateg. Study CAE* **2012**, *14*, 4–9. (In Chinese)
5. Wu, J.; Han, G.; Zhou, H.; Li, N. Economic development and declining vulnerability to climate-related disasters in China. *Environ. Res. Lett.* **2018**, *13*, 034013. [CrossRef]
6. Lei, X. Overview of the development history of China's typhoon research and operational work in the past century. *Sci. China Earth Sci.* **2020**, *50*, 321–338. (In Chinese) [CrossRef]
7. Lei, X.; Chen, P.; Yang, Y.; Qian, Y. Characters and objective assessment of disasters caused by typhoons in China. *Acta Meteorol. Sin.* **2009**, *67*, 875–883. (In Chinese)

8. Shi, J.; Cui, L. Spatial and temporal characteristics of four main types of meteorological disasters in East China. *Atmosfera* **2020**, *33*, 233–247. [CrossRef]
9. Wu, J.; Fu, Y.; Zhang, J.; Li, N. Meteorological Disaster Trend Analysis in China: 1949-2013. *J. Nat. Resour.* **2014**, *29*, 1520–1530. (In Chinese)
10. Xu, W.; Zhuo, L.; Zheng, J.; Ge, Y.; Gu, Z.; Tian, Y. Assessment of the Casualty Risk of Multiple Meteorological Hazards in China. *Int. J. Environ. Res. Public Health* **2016**, *13*, 222. [CrossRef]
11. Chen, L.; Luo, Z.; Li, Y. Research advances on tropical cyclone landfall process. *Acta Meteorol. Sin.* **2004**, *62*, 541–549. (In Chinese)
12. Duan, Y.; Fang, J.; Cheng, Z.; Xu, J.; Li, Q.; Zhan, R.; Qian, C.; Chen, J.; Ren, F. Advances and trends in tropical cyclone research and forecasting: An overview of the ninth World Meteorological Organization International Workshop on Tropical Cyclones (IWTC-9). *Acta Meteorol. Sin.* **2020**, *78*, 537–550.
13. Ma, L. Research Progress on China typhoon numerical prediction models and associated major techniques. *Prog. Geophys.* **2014**, *029*, 1013–1022. (In Chinese)
14. Marchok, T.; Rogers, R.; Tuleya, R. Validation Schemes for Tropical Cyclone Quantitative Precipitation Forecasts: Evaluation of Operational Models for U.S. Landfalling Cases. *Weather. Forecast.* **2007**, *22*, 726–746. [CrossRef]
15. Wang, Y.; Shen, X.-S.; Chen, D.-H. Verification of tropical cyclone rainfall predictions from CMA and JMA global models. *J. Trop. Meteorol.* **2012**, *18*, 537–542.
16. Yu, Z.F.; Chen, Y.J.; Ebert, B.; Davidson, N.E.; Xiao, Y.; Yu, H.; Duan, Y.H. Benchmark rainfall verification of landfall tropical cyclone forecasts by operational ACCESS-TC over China. *Meteorol. Appl.* **2020**, *27*, e1842. [CrossRef]
17. Zhou, J.; Luo, Z. Numerical Study on the Maximum Velocity Reinforcement in Typhoons. *Trans. Atmos. Sci.* **2002**, *25*, 199–206. (In Chinese)
18. Brand, S. Interaction of Binary Tropical Cyclones of the Western North Pacific Ocean. *J. Appl. Meteorol. Climatol.* **1970**, *9*, 433–441. [CrossRef]
19. Dong, K.; Neumann, C.J. On the Relative Motion of Binary Tropical Cyclones. *Mon. Weather. Rev.* **1983**, *111*, 945–953. [CrossRef]
20. Fujiwhara, S. The natural tendency towards symmetry of motion and its application as a principle in meteorology. *Q. J. R. Meteorol. Soc.* **1921**, *47*, 287–292. [CrossRef]
21. Fujiwhara, S. On the growth and decay of vortical systems. *Q. J. R. Meteorol. Soc.* **1923**, *49*, 75–104. [CrossRef]
22. Jang, W.; Chun, H.-Y. Characteristics of Binary Tropical Cyclones Observed in the Western North Pacific for 62 Years (1951–2012). *Mon. Weather. Rev.* **2015**, *143*, 1749–1761. [CrossRef]
23. Lander, M.; Holland, G.J. On the interaction of tropical-cyclone-scale vortices. I: Observations. *Q. J. R. Meteorol. Soc.* **1993**, *119*, 1347–1361. [CrossRef]
24. Lee, J.-D.; Ito, K.; Chan, J.C.L. Importance of self-induced vertical wind shear and diabatic heating on the Fujiwhara effect. *Q. J. R. Meteorol. Soc.* **2023**, *149*, 1197–1212. [CrossRef]
25. Liu, H.-Y.; Gu, J.-F.; Wang, Y. Consistent Pattern of Rainfall Asymmetry in Binary Tropical Cyclones. *Geophys. Res. Lett.* **2023**, *50*, e2022GL101866. [CrossRef]
26. Carr, L.E.; Boothe, M.A.; Elsberry, R.L. Observational Evidence for Alternate Modes of Track-Altering Binary Tropical Cyclone Scenarios. *Mon. Weather. Rev.* **1997**, *125*, 2094–2111. [CrossRef]
27. Carr, L.E.; Elsberry, R.L. Objective Diagnosis of Binary Tropical Cyclone Interactions forthe Western North Pacific Basin. *Mon. Weather. Rev.* **1998**, *126*, 1734–1740. [CrossRef]
28. Ren, F.; Xie, Y.; Yin, B.; Wang, M.; Li, G. Establishment of an Objective Standard for the Definition of Binary Tropical Cyclones in the Western North Pacific. *Adv. Atmos. Sci.* **2020**, *37*, 1211–1221. [CrossRef]
29. Chang, J.C.L.; Lam, H. Performance of the ECMWF Model in Predicting the Movement of Typhoon Wayne (1986). *Weather. Forecast.* **1989**, *4*, 234–245. [CrossRef]
30. Jarrell, J.D.; Brand, S.; Nicklin, D.S. An Analysis of Western North Pacific Tropical Cyclone Forecast Errors. *Mon. Weather. Rev.* **1978**, *106*, 925–937. [CrossRef]
31. Li, H.; Ge, X.; Peng, M.; Li, L. The Influences of Monsoon Trough on the Relative Motion of Binary Tropical Cyclones. *J. Meteorol. Soc. Jpn. Ser. II* **2022**, *100*, 729–749. [CrossRef]
32. Wang, M.; Ren, F.; Xie, Y.; Li, G.; Yang, M.-J.; Feng, T. Characteristics and Causes of Extreme Rainfall Induced by Binary Tropical Cyclones over China. *Asia-Pac. J. Atmos. Sci.* **2021**, *57*, 311–320. [CrossRef]
33. Xu, X.; Lu, C.; Xu, H.; Chen, L. A possible mechanism responsible for exceptional rainfall over Taiwan from Typhoon Morakot. *Atmos. Sci. Lett.* **2011**, *12*, 294–299. [CrossRef]
34. Jang, W.; Chun, H.-Y. Effects of thermodynamic profiles on the interaction of binary tropical cyclones. *J. Geophys. Res. Atmos.* **2015**, *120*, 9173–9192. [CrossRef]
35. Shin, S.-E.; Han, J.-Y.; Baik, J.-J. On the Critical Separation Distance of Binary Vortices in a Nondivergent Barotropic Atmosphere. *J. Meteorol. Soc. Jpn. Ser. II* **2006**, *84*, 853–869. [CrossRef]
36. Wu, C.-C.; Huang, T.-S.; Huang, W.-P.; Chou, K.-H. A New Look at the Binary Interaction: Potential Vorticity Diagnosis of the Unusual Southward Movement of Tropical Storm Bopha (2000) and Its Interaction with Supertyphoon Saomai (2000). *Mon. Weather. Rev.* **2003**, *131*, 1289–1300. [CrossRef]
37. Xu, H.; Duan, Y.; Li, Y.; Wang, H. Indirect Effects of Binary Typhoons on an Extreme Rainfall Event in Henan Province, China From 19 to 21 July 2021: 2. Numerical Study. *J. Geophys. Res. Atmos.* **2022**, *127*, e2021JD036083. [CrossRef]

38. Yang, C.-C.; Wu, C.-C.; Chou, K.-H.; Lee, C.-Y. Binary Interaction between Typhoons Fengshen (2002) and Fungwong (2002) Based on the Potential Vorticity Diagnosis. *Mon. Weather. Rev.* **2008**, *136*, 4593–4611. [CrossRef]
39. Ren, F.; Jia, L.; Wu, C.; Ding, C.; Zhang, D.; Jia, Z.; Ma, Y.; Qiu, W. Advances in dynamic-statistical analog ensemble forecasting and its application to precipitation prediction of landfalling typhoons: A renewed understanding. *Acta Meteorol. Sin.* **2023**, *81*, 193–204. (In Chinese)
40. Ren, F.; Yang, H. An overview of advances in typhoon rainfall and its forecasting researches in China during the past 70 years and future prospects. *Torrential Rain Disasters* **2019**, *38*, 526–540. (In Chinese)
41. Wang, M.; Ding, C.; Ren, F.; Zhang, D.-L.; Jia, L. Heavy Rainfall Forecast of Landfalling Tropical Cyclone Over China with an Upgraded DSAEF_LTP Model. *J. Geophys. Res. Atmos.* **2023**, *128*, e2022JD038192. [CrossRef]
42. Huang, H.; Zhao, Y.; Xun, A.; Chen, J. Causality analysis of difference of heavy rainfall distribution in Fujian caused by typhoons Soulik and Trami along similar tracks in 2013. *Torrential Rain Disasters* **2021**, *40*, 136–146. (In Chinese)
43. Yan, L.; Zhou, Y.; Liu, X.; Huang, Y.; Wang, Y. Comparative analyses of the heavy rainfall associated with landfalling tropical cyclones SOULIK (1307) and MARIA (1808) with similar routes. *Atmos. Res.* **2022**, *271*, 106124. [CrossRef]
44. Yan, L.; Zhou, Y.; Wang, Y. Analysis on Different Characteristics and Causes of Precipitation Distribution during the Landing of Typhoon "Soudelor" (1513) and Typhoon "Matmo" (1410) with Similar Tracks. *Chin. J. Atmos. Sci.* **2019**, *43*, 297–310. (In Chinese)
45. Yu, Z.; Chen, X.; Ni, D.; Ji, C.; Xie, H. Analysis of rainstorms associated with similar track tropical cyclones Haitang (0505) and Bilis (0604). *J. Trop. Meteorol.* **2009**, *15*, 111–115.
46. Bagtasa, G. Analog forecasting of tropical cyclone rainfall in the Philippines. *Weather. Clim. Extrem.* **2021**, *32*, 100323. [CrossRef]
47. Kim, H.-J.; Moon, I.-J.; Kim, M. Statistical prediction of typhoon-induced accumulated rainfall over the Korean Peninsula based on storm and rainfall data. *Meteorol. Appl.* **2020**, *27*, e1853. [CrossRef]
48. Kim, J.-S.; Chen, A.; Lee, J.; Moon, I.-J.; Moon, Y.-I. Statistical Prediction of Typhoon-Induced Rainfall over China Using Historical Rainfall, Tracks, and Intensity of Typhoon in the Western North Pacific. *Remote Sens.* **2020**, *12*, 4133. [CrossRef]
49. Li, Q.; Xu, P.; Wang, X.; Lan, H.; Cao, C.; Li, G.; Zhang, L.; Sun, L. An operational statistical scheme for tropical cyclone induced rainfall forecast. *J. Trop. Meteorol.* **2015**, *21*, 101–110. [CrossRef]
50. Ren, F.; Qiu, W.; Ding, C.; Jiang, X.; Wu, L.; Xu, Y.; Duan, Y. An Objective Track Similarity Index and Its Preliminary Application to Predicting Precipitation of Landfalling Tropical Cyclones. *Weather. Forecast.* **2018**, *33*, 1725–1742. [CrossRef]
51. Wei, C.-C. Wavelet Support Vector Machines for Forecasting Precipitation in Tropical Cyclones: Comparisons with GSVM, Regression, and MM5. *Weather. Forecast.* **2012**, *27*, 438–450. [CrossRef]
52. Wei, C.-C. RBF Neural Networks Combined with Principal Component Analysis Applied to Quantitative Precipitation Forecast for a Reservoir Watershed during Typhoon Periods. *J. Hydrometeorol.* **2012**, *13*, 722–734. [CrossRef]
53. Zhong, Y.; Yu, H.; Teng, W.; Chen, P. A Dynamic Similitude Scheme for Tropical Cyclone Quantitative Precipitation Forecast. *J. Appl. Meteorol. Sci.* **2009**, *20*, 17–27. (In Chinese) [CrossRef]
54. Ying, M.; Zhang, W.; Yu, H.; Lu, X.; Feng, J.; Fan, Y.; Zhu, Y.; Chen, D. An Overview of the China Meteorological Administration Tropical Cyclone Database. *J. Atmos. Ocean. Technol.* **2014**, *31*, 287–301. [CrossRef]
55. Dvorak, V.F. Tropical cyclone intensity analysis and forecasting from satellite imagery. *Mon. Weather. Rev.* **1975**, *103*, 420–430. [CrossRef]
56. Hersbach, H.; Bell, B.; Berrisford, P.; Hirahara, S.; Horányi, A.; Muñoz-Sabater, J.; Nicolas, J.; Peubey, C.; Radu, R.; Schepers, D.; et al. The ERA5 global reanalysis. *Q. J. R. Meteorol. Soc.* **2020**, *146*, 1999–2049. [CrossRef]
57. Ren, F.; Byron, G.; David, E. A numerical technique for partitioning cyclone tropical precipitation. *J. Trop. Meteorol.* **2001**, *17*, 308–313. (In Chinese)
58. Ren, F.; Wang, Y.; Wang, X.; Li, W. Estimating tropical cyclone precipitation from station observations. *Adv. Atmos. Sci.* **2007**, *24*, 700–711. [CrossRef]
59. Lu, X.; Yu, H.; Yang, X.; Li, X. Estimating Tropical Cyclone Size in the Northwestern Pacific from Geostationary Satellite Infrared Images. *Remote Sens.* **2017**, *9*, 728. [CrossRef]
60. Merrill, R.T. A Comparison of Large and Small Tropical Cyclones. *Mon. Weather. Rev.* **1984**, *112*, 1408–1418. [CrossRef]
61. Draxler, R.R. An Overview of the HYSPLIT_4 Modelling System for Trajectories, Dispersion, and Deposition. *Aust. Meteorol. Mag.* **1998**, *47*, 295–308.
62. Draxler, R.R.; Stunder, B.; Rolph, G.; Stein, A.; Taylor, A. *HYSPLIT User's Guide*; National Oceanic and Atmospheric Administration: Washington, DC, USA, 2023.
63. Su, L.; Yuan, Z.; Fung, J.C.H.; Lau, A.K.H. A comparison of HYSPLIT backward trajectories generated from two GDAS datasets. *Sci. Total Environ.* **2015**, *506–507*, 527–537. [CrossRef] [PubMed]
64. Kossin, J.P. A global slowdown of tropical-cyclone translation speed. *Nature* **2018**, *558*, 104–107. [CrossRef] [PubMed]
65. Qiu, W.; Ren, F.; Wu, L.; Chen, L.; Ding, C. Characteristics of tropical cyclone extreme precipitation and its preliminary causes in Southeast China. *Meteorol. Atmos. Phys.* **2019**, *131*, 613–626. [CrossRef]
66. Yamaguchi, M.; Chan, J.C.L.; Moon, I.-J.; Yoshida, K.; Mizuta, R. Global warming changes tropical cyclone translation speed. *Nat. Commun.* **2020**, *11*, 47. [CrossRef] [PubMed]
67. Ding, C.; Su, Z.; Ren, F.; Wong, W.-K.; Chen, B.; Ren, H. Prediction of tropical cyclone precipitation over China by the DSAEF_LTP model. *Q. J. R. Meteorol. Soc.* **2022**, *148*, 2243–2253. [CrossRef]

68. Li, Y.; Chen, L.; Xu, X. Numerical Experiments of the Impact of Moisture Transportation on Sustaining of the Landfalling Tropical Cyclone and Precipitation. *Chin. J. Atmos. Sci.* **2005**, *29*, 91–98. (In Chinese)
69. Gray, W.M.; World Meteorological Organization; Commission for Atmospheric Sciences. *Recent Advances in Tropical Cyclone Research from Rawinsonde Composite Analysis*; WMO: Geneva, Switzerland, 1981.
70. Li, Y.; Chen, L.; Wang, J. The diagnostic analysis on the characteristics of large scale circulation corresponding to the sustaining and decaying of tropical cyclone after it's landfall. *Acta Meteorol. Sin.* **2004**, *62*, 167–179. (In Chinese)
71. Deng, L.; Feng, J.; Zhao, Y.; Bao, X.; Huang, W.; Hu, H.; Duan, Y. The Remote Effect of Binary Typhoon Infa and Cempaka on the "21.7" Heavy Rainfall in Henan Province, China. *J. Geophys. Res. Atmos.* **2022**, *127*, e2021JD036260. [CrossRef]
72. Cheng, J.; You, Q.; Cai, M. Climatic Distribution and Trend Characteristics of Global Cloud Water Content. *Clim. Environ. Res.* **2021**, *26*, 541–555. (In Chinese)
73. Liu, J.; You, Q.; Zhou, Y.; Ma, Q.; Cai, M. Spatiotemporal Distribution and Trend of Cloud Water Content in China Based on ERA-Interim Reanalysis. *Plateau Meteorol.* **2018**, *37*, 1590–1604. (In Chinese)
74. Dai, N.; Xie, A.; Zhang, Y. Interannual and Interdecadal Variations of Summer Monsoon Activities over South China Sea. *Clim. Environ. Res.* **2000**, *5*, 363–374.
75. Rao, C.; Bi, X.; Chen, G.; Yu, Z. A Numerical Simulation on the Impacts of the Offshore Typhoons on Water Vapor Flux, Dynamic and Thermal Conditions of the Extreme Rainstorm Event in Henan Province in July 2021. *Chin. J. Atmos. Sci.* **2022**, *46*, 1577–1594. (In Chinese)
76. Schumacher, R.S.; Galarneau, T.J. Moisture Transport into Midlatitudes ahead of Recurving Tropical Cyclones and Its Relevance in Two Predecessor Rain Events. *Mon. Weather. Rev.* **2012**, *140*, 1810–1827. [CrossRef]
77. Schumacher, R.S.; Galarneau, T.J.; Bosart, L.F. Distant Effects of a Recurving Tropical Cyclone on Rainfall in a Midlatitude Convective System: A High-Impact Predecessor Rain Event. *Mon. Weather. Rev.* **2011**, *139*, 650–667. [CrossRef]
78. Chien, F.-C. A Numerical Study on the Slow Translation Speed of Typhoon Morakot (2009). *SOLA* **2014**, *10*, 190–193. [CrossRef]
79. Chien, F.-C.; Kuo, H.-C. On the extreme rainfall of Typhoon Morakot (2009). *J. Geophys. Res. Atmos.* **2011**, *116*, 15092. [CrossRef]